Modelling of the Dendritic Crystallization by the Cellular Automaton Method

A. Zyska*, Z. Konopka, M. Łągiewka, M. Nadolski
Foundry Department, Czestochowa University of Technology,
Al. Armii Krajowej 19, 42-200 Częstochowa, Poland
*Corresponding author. E-mail address: zyska@wip.pcz.pl

Abstract

A numerical model of binary alloy crystallization, based on the cellular automaton technique, is presented. The model allows to follow the crystallization front movement and to generate the images of evolution of the dendritic structures during the solidification of a binary alloy. The mathematic description of the model takes into account the proceeding thermal, diffusive, and surface phenomena. There are presented the results of numerical simulations concerning the multi-dendritic growth of solid phase along with the accompanying changes in the alloying element concentration field during the solidification of Al + 5% wt. Mg alloy. The model structure of the solidified casting was achieved and compared with the actual structure of a die casting. The dendrite interaction was studied with respect to its influence on the generation and growth of the primary and secondary dendrite arms and on the evolution of solute segregation both in the liquid and in the solid state during the crystallization of the examined alloy. The morphology of a single, free-growing dendritic crystal was also modelled. The performed investigations and analyses allowed to state e.g. that the developed numerical model correctly describes the actual evolution of the dendritic structure under the non-equilibrium conditions and provides for obtaining the qualitatively correct results of simulation of the crystallization process.

Keywords: Numerical modelling, Crystallization, Cellular automata, Binary alloys, Structure modeling

1. Introduction

Cellular automata (CA) can be applied for modelling the structure within a whole casting [1,2] or within its part [3-15]. In the first case, the texture across the wall and changes in grain size are modelled, while in the second one – the morphology of individual crystals is predicted. The general idea of models determined for the whole volume of a casting is similar to the micro-macro models. The cellular automaton method is applied for modelling of nucleation and grain growth, as well as for the calculating the quantity of the transformed phase, while the heat transfer is modelled in macroscopic scale on the basis of the energy equation. There is a cross-coupling between both distinguished scales, the micro and the macro ones. The

calculation results taken from the cellular automaton are used to solve the thermal problem, and the temperature field determined in macro-scale is interpolated and the resulting values are assigned to the individual cells of the automaton. Such a solution was presented for the first time in the Reference [1], where the cellular automaton method was combined with the finite element method. The professional literature often uses the acronym CAFE for this type of models, or describes them more generally as multi-scale or hybrid models.

The modelling of morphology of the primary crystals is based on the fundamental principles of the theory of crystallization of metals and alloys. The generation of shapes of the growing structures proceeds by modelling the movement of the phase boundary in the automaton cells of dimensions of the 1 μm order. A characteristic feature of this approach is that the model takes

into account parameters describing the crystallization front: its curvature, anisotropy, energy and undercooling. The heat transfer equation, the diffusion equation, and sometimes the equation of movement of the liquid metal, are solved at the meso-scale level. Furthermore, any crystal nucleation mechanism can be adopted into the cellular automaton. Including all the mentioned phenomena in one model allows to reproduce to a large extent the actual non-equilibrium crystallization conditions. Calculations give the possibility to follow the sprouting and the evolution of dendrite arms of the first and the subsequent orders in dendrites or the close-coupled growth of phases during the eutectic crystallization, taking into account the interactions between the growing crystallites. It is possible to get information about the topology of the modelled structures and about the micro-segregation of the alloying elements both in the liquid and in the solid phase [3-7, 12-15].

To realize the numerical simulation in the CA meso-model, the examined area is divided with a regular square grid into elementary cells, and a series of values related to the solidification process is ascribed to the each cell. The automaton cells can be in one of the three phase states: 0 – liquid phase, 1 – solid phase, or (0÷1) – interface. For each cell, the subsequent calculation steps include finding changes in temperature and solute concentration, and for two-phase cells also the determination of the growth rate, the solid phase increment, the current phase boundary curvature, the surface tension anisotropy, and the equilibrium liquidus temperature. Scanning of cells is performed on the basis of Moore or von Neumann neighbourhoods for blocks of elementary cells 3×3 or 5×5 in size. At the moment when the fraction of solid phase in a cell reaches 1, its state is changed to solid, and the neighbouring cells in liquid state are attached to the interface, inheriting the initial crystallographic orientation, the attachment to the same grain, etc. The momentary local shape of the crystallization front is reproduced, and the evolution of the alloy structure is simulated with accuracy to the size of the automaton cell. The modelling is usually performed for the *2D* regions [3-7, 10-15], but the development of the *3D* models can be seen during recent years [8, 9].

The present paper describes a portion of the comprehensive study covering problems of modelling the solidification and the crystallization of castings, in which one of the partial objectives was the development of the numerical model and, subsequently, the algorithm based on the cellular automaton technique, which would allow to observe the movement of the crystallization front and to generate the images of evolution of the dendritic structures during the solidification of a binary alloy.

2. Construction of the cellular automaton

The cellular automaton was constructed on a planar region divided with the regular square grid into elementary cells of side length equal to a. The computational domain was represented by a square $N \times N$ matrix. The state of each cell was described by variables of either continuous or discrete character, each type with its corresponding domain. The following basic values were defined within the cellular automaton lattice: concentration of the

alloying element (the solute) – C, temperature – T, fraction of the solid phase – g_s, phase state – F, preferential crystallographic orientation angle – θ_0, the attachment to the grain – Z_N, the direction normal to the phase boundary – φ, the curvature of the phase boundary – K.

Two types of neighbourhood were adopted in the modelling process. The von Neumann neighbourhood was applied for the mass and energy transport phenomena, while the Moore neighbourhood based on 3×3 cell array was used for all other cases. Authors' own transition rules were introduced into the description of the dendritic structure evolution in order to restrict the artificial anisotropy of the CA lattice. The procedure of attaching the neighbouring cells to the interface is presented in Ref. [15]. At the edges of the cellular automaton grid the periodic or the reflective boundary conditions were determined. They were applied for determination of all the mentioned values and for solving all equations, including the diffusion and the heat transfer equations. Also the second-type boundary condition was assumed for the thermal problem.

The basis of the applied cellular automaton consists of the three fields: the temperature field, the solute concentration field, and the solid phase fraction field. They reproduce the kinetics of the dendritic structure growth both in the quantitative and the qualitative aspects. The momentary position of the crystallisation front and the momentary shape of dendrites is obtained by the coupled solution of the model equation system.

It was assumed in the automaton concept that the growth of dendrites is controlled by the rate of solute diffusion away from the crystallisation front. The growth is driven by the deviation from the equilibrium state, and its measure is the difference between the local momentary equilibrium solute concentration and the local momentary chemical composition of the liquid phase. The equilibrium chemical composition results from the thermodynamic relationship between the liquidus temperature and the curvature of the crystallization front. The momentary temperature field and the shape of the front (convex, flat, or concave) determine the momentary distribution of the equilibrium concentration in the interface cells, while the concentration gradient generated ahead of the crystallization front is decisive with respect to the growth rate of the solid phase.

The solute transport in the liquid and solid phases, as well as in the interface cells, is described by the two-dimensional diffusion equation, which was approximated using the formula:

$$\Delta C_{i,j} = \frac{\Delta t}{\Delta x^2}\left[\sum_{Ne=1}^{4} D_{ef,Ne}\left(C_{L,Ne}^{t} - C_{L,i,j}^{t}\right)\right] \qquad (1)$$

where: $\Delta C_{i,j}$ – solute concentration change in the (i, j) cell during the Δt time, $C_{L,i,j}^{t}$, $C_{L,Ne}^{t}$ – solute concentration in the (i, j) cell and in the cells of its von Neumann neighbourhood at the time t, $\Delta x = \Delta y = a$ – lattice constant.

The D_{ef} coefficient occurring in the Equation (1) depends on the configuration of the neighbouring cells (in terms of the von Neumann neighbourhood) at the time t and is determined by the following formulas:

$$D_{ef} = \begin{cases} D_L & dla \ (g_{S,i,j} < 1) \ i \ (g_{S,Ne} = 0) \\ k_0 D_S & dla \ (g_{S,i,j} > 0) \ i \ (g_{S,Ne} = 1) \\ 0.5(D_L + D_S) & dla \ (0 < g_{S,i,j} < 1) \ i \ (0 < g_{S,Ne} < 1) \\ 0 & dla \ \left[(g_{S,i,j} = 1) \ i \ (g_{S,Ne} = 0)\right] \ lub \ \left[(g_{S,i,j} = 0) \ i \ (g_{S,Ne} = 1)\right] \end{cases} \quad (2)$$

where: k_0 – solute partition coefficient, D_L – solute diffusion coefficient in the liquid phase, D_S – solute diffusion coefficient in the solid phase, $g_{S,i,j}$, $g_{S,Ne}$ – fractions of the solid and the liquid phases, respectively, in the (i,j) cell and in cells belonging to the von Neumann neighbourhood.

The above expression allows to describe the solute diffusion between two interface cells being both in the liquid or both in the solid state. It includes also the mixed neighbourhoods, i.e. the interface/liquid phase or the interface/solid phase ones. In such cases the interface cell is regarded as liquid at the edge contacting with the liquid phase, while at the edge contacting with the solid phase it is considered as totally solidified. The lack of diffusion is assumed in the case of the liquid/solid phase neighbourhood.

The increment of the solid phase in the transition cells is calculated from the equation of mass balance, which after differentiation (with respect to time) and approximation with the difference quotient takes the form:

$$k_0 C_{L,i,j}^t \Delta g_{S,i,j} + k_0 (C_{L,i,j}^{t+1} - C_{L,i,j}^t) g_{S,i,j}^t - C_L^t \Delta g_{S,i,j} +$$
$$(C_{L,i,j}^{t+1} - C_{L,i,j}^t)(1 - g_{S,i,j}^t) = \Delta C_{i,j} \quad (3)$$

The calculation proceeds in two stages. After solving the diffusion equation, it is assumed for the first step that the solid phase in the transition cells does not grow ($\Delta g_S=0$, initial pseudo-condition) and only the solute diffusion away of the interface is in progress. As a result, the solute concentration decreases to the value of:

$$C_{L,i,j}^{t+1,pseudo} = C_{L,i,j}^t + \frac{\Delta C_{i,j}}{1 + g_{S,i,j}^t (k_0 - 1)} \quad (4)$$

Then it is checked which of the interface cells exhibit the concentration $C_{L,i,j}^{t+1,pseudo}$ lower than the equilibrium concentration $C_{L,i,j}^F$. For cells where the condition $C_{L,i,j}^{t+1,pseudo} < C_{L,i,j}^F$ is fulfilled, the value of the equilibrium concentration $C_{L,i,j}^{t+1} = C_{L,i,j}^F$ is assumed and the increment of the solid phase is calculated from the expression (3), by transforming it to the form:

$$\Delta g_{S,i,j} = \frac{\Delta C_{i,j} - (C_{L,i,j}^F - C_{L,i,j}^t)[1 + g_{S,i,j}^t (k_0 - 1)]}{C_{L,i,j}^t (k_0 - 1)} \quad (5)$$

The concentration is $C_{L,i,j}^{t+1} = C_{L,i,j}^{t+1,pseudo}$ for all other interface cells. The Formula (4) can be applied also for calculation of the momentary solute concentration in solid phase and liquid phase cells, by substituting $g_S = 0$ and $g_S =1$, respectively.

The equilibrium concentration at the crystallization front occurring in the Equation (5) was calculated from the formula:

$$C_L^F = C_0 + \frac{T^F - T_L}{m_L} + \frac{\Gamma K \{1 - \delta \cos[m_S(\varphi - \theta_0)]\}}{m_L} \quad (6)$$

where: C_0 – solute concentration in the alloy, T_L – liquidus temperature, T^F – temperature at the crystallization front, m_L – the slope of the liquidus line, Γ – Gibbs-Thomson coefficient, K – curvature of the crystallization front, m_s – order of the crystal symmetry, for crystals with cubic lattice $m_s = 4$, δ – coefficient dependent on the amplitude of changes of the surface tension and on the symmetry of the crystal, φ – the angle between the growth direction (the normal to the crystallization front) and the reference direction ($0x$ coordinate axis), θ_0 – the angle between the preferential crystallographic direction and the reference direction.

The above equation allows to take into account the Gibbs-Thomson effect – the influence of the crystallization front configuration on the change of solute equilibrium concentration in the interface cells. Both the direction normal to the crystallization front and the curvature of the front should be known to solve the Equation (6). The first of these quantities was found by employing the method of a mass centre of a block of cells considered as the immediate neighbourhood. In this method, the direction normal to the crystallisation front is defined by the unit vector anchored at the centre of mass of the block of cells 3×3 in size, and directed toward the centre of the central cell. The coordinates of the block mass centre (x_s, y_s) are calculated from the sum of inertia moments of individual masses, while the appropriate solid phase fractions stand for masses of the individual cells.

$$x_S = \frac{M_y}{g_S^B} = \frac{\sum_{i=1}^{6} g_{S,i}^x \Delta y}{\sum_{i=1}^{9} g_{S,i}} \quad (7)$$

$$y_S = \frac{M_x}{g_S^B} = \frac{\sum_{i=1}^{6} g_{S,i}^y \Delta x}{\sum_{i=1}^{9} g_{S,i}} \quad (8)$$

where: M_x, M_y – moments of the system with respect to the $0x$ and $0y$ axes, respectively, g_S^B – fraction of the solid phase within the 3×3 block of cells, $g_{S,i}^x$ – fractions of solid phase in cells g^{NE}, g^E, g^{SE}, g^{NW}, g^W, g^{SW}, $g_{S,i}^y$ – fractions of solid phase in cells g^{NW}, g^N, g^{NE}, g^{SW}, g^S, g^{SE}, the superscripts being related to the position of cells named according to the compass rose.

The angle between the direction normal to the phase boundary and the reference direction ($0x$) was calculated from the relationship:

$$\varphi = \arctan\left(\frac{M_x}{M_y}\right) \quad (9)$$

The curvature of the solidification front was derived from the partial derivatives of the first and the second order, employing the relationship proposed by Kothe [10]:

$$K = \frac{2\frac{\partial g_s}{\partial x}\frac{\partial g_s}{\partial y}\frac{\partial^2 g_s}{\partial x \partial y} - \left(\frac{\partial g_s}{\partial x}\right)^2 \frac{\partial^2 g_s}{\partial y^2} - \left(\frac{\partial g_s}{\partial y}\right)^2 \frac{\partial^2 g_s}{\partial x^2}}{\left[\left(\frac{\partial g_s}{\partial x}\right)^2 + \left(\frac{\partial g_s}{\partial y}\right)^2\right]^{3/2}} \quad (10)$$

The Equation (1) was solved by the method of elementary balances, which – for the applied square CA lattice – is equivalent to the MRS method. The adopted explicit numerical scheme is characterised by the limited stability, which – for the case of cellular automata with lattice constant a of the order of 10^{-6} m – demands for applying a small time step. The stability of the numerical method was determined from the condition [4, 6]:

$$\frac{D_L \Delta t^C}{\Delta x^2} < 0,25 \quad (11)$$

The above condition along with the restriction concerning the maximum growth rate of the solid phase in the interface cells was used in the procedure of the time step optimization:

$$\Delta t_{stab} = \min\left(0,25\frac{\Delta x^2}{D_L}; 0,02\frac{\Delta x}{\upsilon_n^{max}}\right) \quad (12)$$

where: υ_n^{max} – maximum value of the growth rate normal to the crystallization front in the interface cells.

The solution of the thermal problem with the use of the cellular automaton grid is numerically not effective if the explicit schemes are applied. It results from the low stability of these methods, which under the condition of [5, 11]:

$$\frac{\lambda \Delta t^T}{\Delta x^2 c\rho} < 0,25 \quad (13)$$

where: λ – thermal conductivity, c – specific heat, ρ – density, are restricted with the time step Δt_{stab} at the level of 10^{-9} s (exemplary value for the aluminium alloys, the lattice constant $a = 10^{-6}$ m). Such a value is smaller by four orders in comparison with the restrictions imposed while solving the diffusion equation in the explicit scheme (11). To avoid this inconvenience some of the models [4, 12-14] employ the implicit method or assume the time-dependent, but uniform temperature for the whole computational domain. Another way of reducing the computation time, used in the present work, is the determination of temperature field by means of the multigrid method. Double discretisation was applied to the considered area – a coarse secondary lattice was superimposed on the main CA lattice. The lattice constant for the secondary grid (Δx_{RZ}) is many times greater than the size a of the elementary cell. A block of cells in the main lattice, of dimensions $n_B \times n_B$, is equivalent to the elementary cell of the coarse lattice. The cross-coupling occurs between the two lattices. For every

time step the energy equation is solved in the coarse lattice and the resulting temperature field is interpolated to the main CA grid. The increments of the solid phase, in turn, are summarized in blocks and the sums assigned to the coarse lattice.

The heat exchange in the region discretised with the coarse grid was described by the two-dimensional Fourier-Kirchhoff equation and approximated with the explicit scheme:

$$T_{i,j}^{t+1} = T_{i,j}^t + \frac{\Delta t}{\Delta x_{RZ}^2}\left[\sum_{Ne=1}^{4}\overline{a}_{RZ,Ne}(T_{Ne} - T_{i,j})\right] + \frac{L}{\overline{c}}\frac{\sum \Delta g_s}{n_B^2} \quad (14)$$

where: $T_{i,j}^{t+1}$ – a new value of temperature in the (i, j) cell of the coarse lattice at the time $t+1$, $T_{i,j}^t, T_{Ne}$ – the temperature in the (i, j) cell and in the cells of the von Neumann neighbourhood in the coarse lattice at the time t, L – solidification heat, $\overline{c}$ – the average specific heat, $\sum \Delta g_s$ – the sum of solid phase increments within a block of cells of the main lattice, n_B^2 – the number of cells constituting the block.

The value of $\overline{a}_{RZ,Ne}$ quantity occurring in the Equation (15) was calculated as the harmonic mean of the thermal diffusivities of the central cell (i, j), denoted $a_{RZ,i,j}$, and the neighbouring cells, $a_{RZ,Ne}$:

$$\overline{a}_{RZ,Ne} = \frac{2a_{RZ,i,j}a_{RZ,Ne}}{a_{RZ,i,j} + a_{RZ,Ne}} \quad (15)$$

The value of thermal diffusivity for the individual cells of the coarse lattice was approximated according to the rule of mixtures:

$$a_{RZ} = a_S g_{RZ} + a_L(1 - g_{RZ}) \quad (16)$$

where: a_S, a_L – thermal diffusivities for the solid and the liquid phases, respectively, g_{RZ} – fraction of the solid phase in cells of the coarse lattice:

$$g_{RZ} = \frac{\sum g_s}{n_B^2} \quad (17)$$

The rule of mixtures was applied also for the determination of the average specific heat of the alloy.

The interpolation of the temperature field to the automaton main grid was performed by applying the procedure of the progressive lattice refining, passing from the far-distant neighbours to the close-positioned ones [15].

The work is focused mainly on the description of the growth of dendritic structures, therefore the problem of nucleation was dealt with in a simplified manner. The number of *nucleation cells* N_Z within the computational domain was set on the basis of the quadratic formula, often used in the macroscopic description of solidification, concerning the instant nucleation [16]:

$$N_Z = a_Z + b_Z \left(\frac{dT}{dt}\right)^2_{sr} \qquad (18)$$

where: a_Z , b_Z – experimentally found constant coefficients of nucleation, $(dT/dt)_{sr}$ – average cooling rate counted from the beginning of the process to the moment of achieving the T_L temperature.

The angle of the preferential crystallographic orientation $\boldsymbol{\theta_0}$ and the number of grain $\boldsymbol{Z_N}$ are assigned to every *nucleation cell* introduced into the CA domain. These features are ascribed according to the randomization procedures, and they are being inherited by the cells attached to the interface during the automaton evolution.

3. Results of numerical simulations

Modelling of the growth of dendritic crystals was performed for the Al + 5% wt. Mg alloy. The model alloy was chosen because it undergoes the dendritic solidification, is characterised by wide solidification temperature range, and occupies a place relatively far from the beginning of the eutectic transformation in the phase equilibrium diagram. Moreover, it produces a single-phase structure under the equilibrium conditions, and magnesium is easily soluble in its α solid solution. Linearized Al-Mg phase equilibrium diagram is shown in Fig. 1, and the values of parameters applied in calculations are gathered in Table 1.
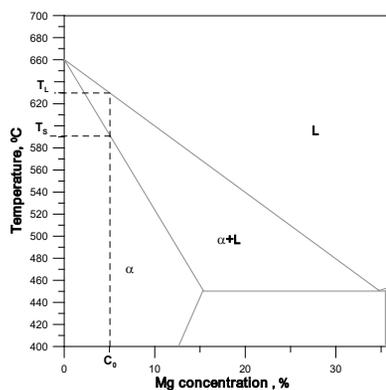
Fig. 1. Al-Mg phase equilibrium diagram

Computer simulations were performed in order to verify the correctness of the developed numerical model and to assess the interaction of dendrites during the generation and growth of the primary and secondary branches in the crystallizing binary alloy. The investigations culminated in achieving the model of the fully solidified casting and in comparing it with the real structure of the AlMg5 alloy. Calculations were performed within the area 608×608 μm^2, employing a cellular automaton of size *304×304*. The boundary conditions for the thermal problem were assumed as follows: the periodic conditions were assumed for the upper and the lower edges, the second-type boundary condition with the heat flux value of $q_b = 70000\ W/m^2$ was adopted at the left edge,

and the thermal symmetry $q_b = 0$ was applied for the right edge. The average rate of the temperature fall, assuming no heat sources exist within the analysed area, was equal to 35 K/s. The diffusion equation was solved for periodic boundary conditions at the upper and the lower edge, and the reflective condition (mass flux $j_b = 0$) at the left and the right edges. After reaching the liquidus temperature, the number of *nucleation cells* was found on the basis of the relationship (18) and they were introduced into the computational domain at random positions.

Table 1.
Material parameters of the model alloy [13, 17, 18]

Parameter	Designation	Value	Unit
Specific heat			
in the liquid phase	c_L	1170	J/(kg·K)
in the solid phase	c_S	1100	
Density			
in the liquid phase	ρ_L	2350	kg/m^3
in the solid phase	ρ_S	2550	
Thermal conductivity			
in the liquid phase	λ_L	90	W/(m·K)
in the solid phase	λ_S	170	
Solidification heat	L	390	kJ/kg
Equilibrium partition coefficient	k_0	0,437	–
Slope of the liquidus line	m_L	–5.97	K
Diffusivity			
in the liquid phase	D_L	$2,5\cdot10^{-9}$	m^2/s
in the solid phase	D_S	$4\cdot10^{-11}$	
Gibbs-Thomson coefficient	Γ	$2\cdot10^{-7}$	m·K
Degree of surface tension anisotropy	δ	0,3	–

Table 2 presents the growth sequence of the dendritic structures and the accompanying momentary solute concentration fields in the liquid, the solid, and the transition phases. The interface cells present the average values of Mg concentration, which result from the mass balance. Figure 2 compares the final image of structure resulting from the numerical simulation and the actual structure of a die-cast casting made of the AlMg5 alloy.

The results of the numerical simulation indicate that the changes in the shape of dendrites strongly depend on the interaction of the concentration fields, the growth direction of the primary and secondary dendrite arms, and the initial arrangement of the *nucleation cells* within the computational domain. During the initial period (Table 2, a-c), the main dendrite arms grow from the *nucleation cells*, being surrounded by the arising diffusive layers. The solute concentration at the solidification front increases rapidly and reaches the value of about 6% Mg. At this concentration level, further longitudinal and transversal growth of the main dendrite arms proceeds, and its thermal effect can be seen as the slight temperature recalescence on the cooling curve (see Fig. 3). Next the secondary branches are initiated, and the main dendrite arms come close to one another. The solute concentration fields originated in the liquid begin to interact, and this influences the further growth of both main and secondary arms. The liquid is quickly enriched in the alloying element in

the regions where solidification fronts approach one another, and the diffusion is restricted in some directions. The intensity of drawing the solute away into the melt decreases, and as a result the growth of the main dendrite arms is retarded. Both the shape and the size of the already generated dendrites depends on the initial arrangement of the *nucleation cells* and the growth direction (the angle of preferential crystallographic orientation).

The largest arms are exhibited by dendrites, which nuclei were initially very far apart from other ones, and their orientation angle provided for the longest time of free growth. A small distance between the nuclei cause that the concentration fields interact already at the beginning of solidification and some branches develop only to a very limited extent. The restriction of longitudinal dendrite growth contributes both to the growth of the secondary dendrite arms and to the coarsening of the primary branches. Such a way of solid phase growth is characteristic for the middle stage of AlMg5 alloy solidification.

Table 2.
Momentary Mg concentration fields and the growth sequence of the dendritic crystals
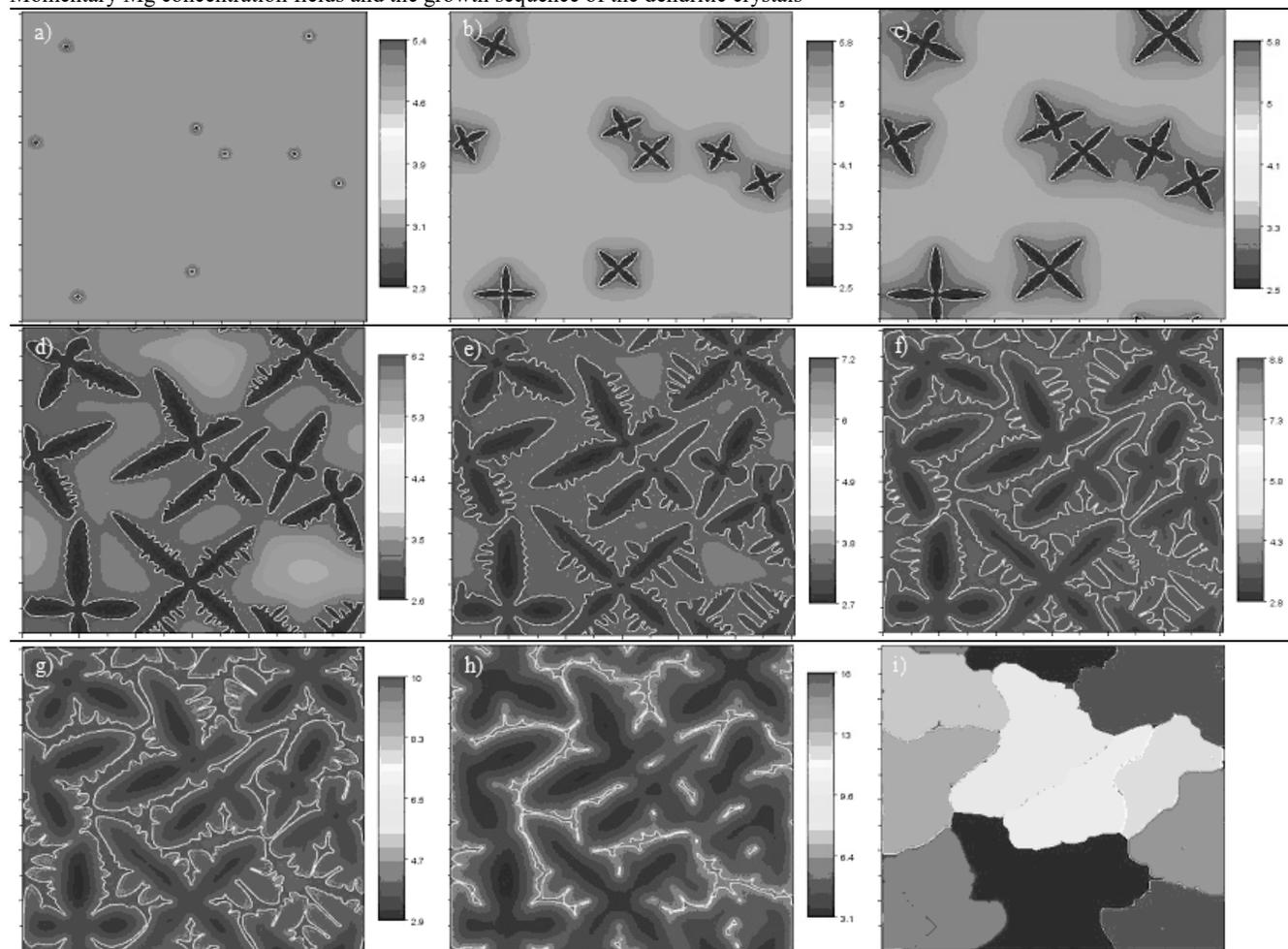
the fraction of solid phase: a) 0.002, b) 0.05, c) 0.1, d) 0.3, e) 0.5, f) 0.7, g) 0.8, h) 0.95
i) the image generated on the basis of grain numbers after the solidification

Similarly to the previous considerations, the interaction of the solute concentration fields promotes the development of these of the secondary branches, which can grow freely in the direction of regions with the lowest solute concentration. The position of crystals and the concentration distribution in some regions create conditions facilitating the development of the ternary branches. However, when main dendrite arms are close and parallel to one another, their evolution proceeds in a different way. In such a case the secondary arms are not developed, and the crystal growth proceeds by coarsening.

At this stage of solidification the superimposed concentration fields result in the decreased solute segregation in the liquid phase. On the contrary, the segregation phenomenon is intensified within the solid phase – an increase in dendrite cross-sectional dimensions results in an increase in the diffusion distance. The highest magnesium concentration occurs in cells close to the crystallization front, and the lowest in regions located along the

main dendrite axes. As the solidification proceeds further, the magnesium distribution in solid phase differs more and more from the equilibrium state. In the final period of solidification, the coagulation of the binary branches takes place, the crystal boundaries come close to other ones, being separated only by a thin layer of the liquid phase enriched greatly in the alloying element.
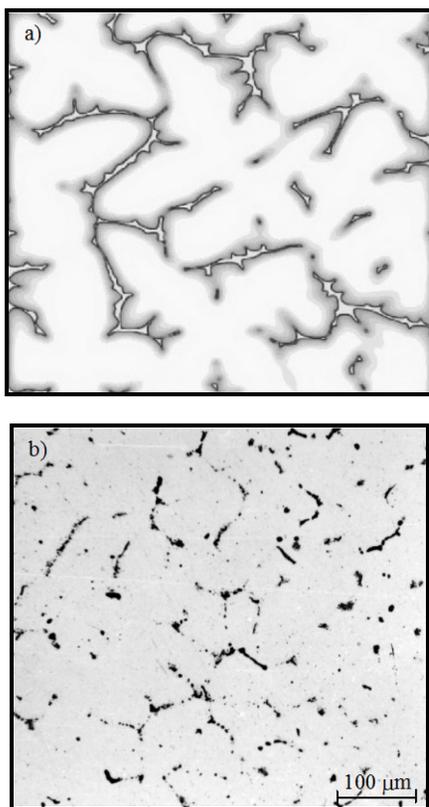
Fig. 2. Structure of AlMg5 alloy: a) modelled – the final stage of solidification, b) actual in the die casting

Magnesium concentration in liquid at the end of the solidification is four times as much as its concentration at the beginning of the process. The reason for such a great Mg concentration value is the non-equilibrium distribution of the solute in solid state, the difference being intensified as the solidification proceeds. The solute segregation (the minimum and the maximum concentration values) in solid state versus the solid phase fraction (g_s) is presented in Figure 4. This figure illustrates also the chemical non-uniformity of the liquid. The segregation phenomenon in the liquid state exhibits the contrary behaviour. The difference in Mg concentration in liquid is the greatest at the beginning of the solidification and gradually decreases to such a level that at the end of the solidification the liquid can be practically regarded as being uniform.

The non-equilibrium solidification described by the model equation system can be compared with the simple model of the equilibrium solidification and with the Scheil model. Figure 5 depicts the changes in Mg concentration at the crystallization front versus the solid phase fraction for both the developed

numerical model and analytical models. The location of $C^F(g_s)$ curve indicates that the average solute concentration at the crystallization front takes more or less the middle value from the range limited by the equilibrium and the extremely non-equilibrium (diffusion precluded in solid state) concentration values.
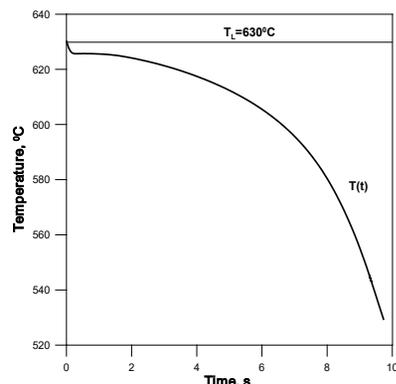
Fig. 3. The solidification curve of the model alloy
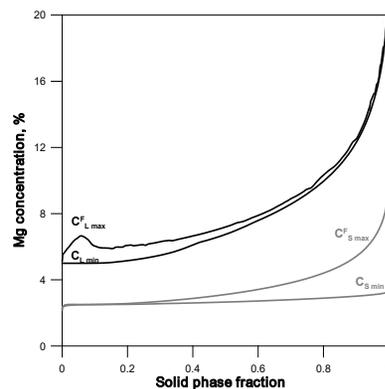
Fig. 4. Magnesium segregation in the liquid and the solid state during solidification
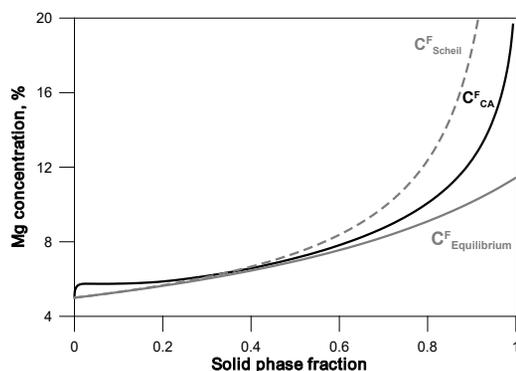
Fig. 5. Changes in Mg concentration at the crystallization front versus the solid phase fraction for the developed numerical model, the equilibrium model, and the Scheil model

Figure 6 presents the morphology of a single dendritic crystal during its free growth. The structure modelled under such crystallization conditions exhibits natural physical anisotropy.

The dendrite has symmetrically arranged lateral branches inclined at an angle of 90° to the main arms. The primary branches increase their transversal dimensions only in the region of stable growth close to the dendrite tip. Secondary arms grow beneath this region and suppress the further growth coarsening of the main branches. As a result, the cross-section of main arms is uniform along the dendrite length. The dendrite tips exhibit also the characteristic surface projections – the sprouts of secondary dendrite branches.
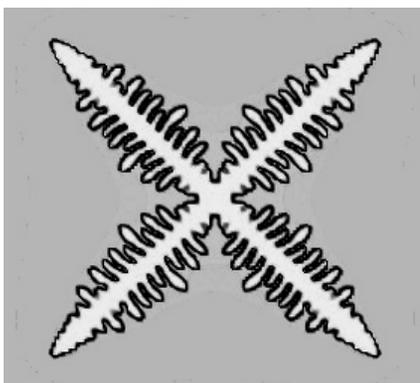
Fig. 6. Shape of dendrite of the orientation angle $\theta_0 = 45°$

4. Final conclusions

1. The developed numerical model, taking into account the kinetics of the diffusion, thermal, and surface phenomena, describes correctly the actual evolution of dendritic structure under the non-equilibrium conditions and provides for obtaining the qualitatively correct results of simulation of the crystallization process.
2. The algorithm based on the cellular automaton technique makes it possible to generate the growth sequence of the dendritic crystals during the solidification and thus get the prognosis of the structure of the solidified casting along with the solute segregation assessment.
3. The developed model can be applied for the analysis of the non-equilibrium solidification of either binary single-phase alloys or the phases crystallizing prior to the eutectic solidification in multi-phase alloys.

References

[1] Gandin, Ch.A. & Rappaz, M. (1994). A coupled finite element cellular automaton model for the prediction of dendritic grain structures in solidification processes. *Acta Metallurgica et Materialia. 42*, 2233-2246.
[2] Gandin, Ch.A., Desbiolles, J.L., Rappaz, M. & Thevoz, Ph., (1999). A Three-Dimensional Cellular Automaton–Finite Element Model for the Prediction of Solidification Grain Structures. *Metallurgical and Materials Transactions A. 30*, 3153-3165.
[3] Beltran-Sanchez, L. & Stefanescu, D.M. (2003). Growth of Solutal Dendrites: A Cellular Automaton Model and Its Quantitative Capabilities. *Metallurgical and Materials Transactions A. 34*, 367-382.
[4] Kuangfei, W., Shan, L., Guofa, M., Changyun, L. & Hengzhi, F. (2010). Simulation of microstructural evolution in directional solidification of Ti-45at.%Al alloy using cellular automaton method. *China Foundry. 7*, 47-51.
[5] Zhu, M.F. & Stefanescu, D.M. (2007). Virtual front tracking model for the quantitative modeling of dendritic growth in solidification of alloys. *Acta Materialia. 55*, 1741-1755.
[6] Michelic, S.C. & Thuswaldner, J.M. (2010). Polydimensional modelling of dendritic growth and microsegregation in multicomponent alloys. *Acta Materialia. 58*, 2738-2751.
[7] Zhu, M.F., Dai, T., Lee, S.Y. & Hong, Ch.P. (2008). Modeling of solutal dendritic growth with melt convection. *Computers and Mathematics with Applications. 55*, 1620 – 1628.
[8] Wie, L., Lin, X., Wang, M. & Huang W. (2012). Orientation selection of equiaxed dendritic growth by three-dimensional cellular automaton model. *Physica B. 407*, 2471-2475.
[9] Zhang, X., Zhao, J., Jiang, H. & Zhu, M. (2012). A three-dimensional cellular automaton model for dendritic growth in multi-component alloys. *Acta Materialia. 60*, 2249-2257.
[10] Kothe, D.B., Mjolsness, R.C. (1991). A Computer Program for Incompressible Flows with Free Surface. Los Alamos National Lab. Los Alamos.
[11] Yin, H., Felicelli, S.D. & Wang, L. (2011). Simulation of a dendritic microstructure with the lattice Boltzmann and cellular automaton methods. *Acta Materialia. 59*, 3124-3136.
[12] Burbelko, A. (2004). *Mezomodeling of Solidification Using a Cellular Automaton*. Monograph UWN-D AGH. Krakow. (in Polish).
[13] Zhu, M.F., Cao, W., Chen, S.L., Hong, C.P. & Chang, Y.A. (2007). Modeling of Microstructure and Microsegregation in Solidification of Multi-Component Alloys. *Journal of Phase Equilibria and Diffusion. 28*, 130-138.
[14] Zhan, X., Wie, Y. & Dong, Z. (2008). Cellular automaton simulation of grain growth with different orientation angles during solidification process. *Journal of Materials Processing Technology. 208*, 1-8.
[15] Zyska, A. (2014). *Modelling of the dendritic structure and the solidification process for a binary alloy*. Monograph WWIPiTM P.Cz. Częstochowa. (in Polish).
[16] Stefanescu, D.M. (2009). *Science and Engineering of Casting Solidification*. Springer.
[17] The thermo-physical database of Nova Flow&Solid program.
[18] Yan, X., Chen, S., Xie, F. & Chang, Y.A. (2002). Computational and Experimental Investigation of Microsegregation in an Al-rich Al-Cu-Mg-Si Quaternary Alloy. *Acta Materialia. 50*, 2199-2207.